

Update for PR05-108: G^0 Experiment Backward Angle
Measurement at $Q^2=0.23 \text{ GeV}^2$

The G^0 Collaboration

California Institute of Technology, Carnegie-Mellon University, College of William and Mary, Grinnell College, Hampton University, L'Institut de Physique Nucléaire d'Orsay, Laboratoire de Physique Subatomique et de Cosmologie Grenoble, Louisiana Tech. University, New Mexico State University, Thomas Jefferson National Laboratory, TRIUMF, University of Illinois at Urbana-Champaign, University of Kentucky, University of Manitoba, University of Maryland, University of Northern British Columbia, University of Winnipeg, Virginia Tech, and Yerevan Physics Institute

December 5, 2005

In response to the proposal PR 05-108 (G^0 backward angle measurements, [1]) presented at PAC 28, the PAC has asked the G^0 collaboration to provide further information concerning both (1) the overall strategy of the PV measurements proposed at the meeting and their potential impact to make definitive determinations of the strange form factors of the nucleon and (2) some technical aspects of the G^0 experiment at $Q^2=0.23$ (GeV/c)². The physics strategy of the PV measurements at JLab has been developed jointly by the G^0 and the HAPPEX collaborations in a letter sent to L. Cardman and the PAC members in October 2005 (with subsequent approval from the PAC). Therefore, this document deals only with the technical aspects of the low Q^2 measurement. The charge from the PAC report is :

The TAC raised a number of technical issues concerning installing, commissioning, and running the G^0 low-energy back-angle experiment. In order to address these issues, the collaboration is asked to work with the Laboratory to develop:*

1. *A well motivated table of beam requirement including halo, helicity-correlated modulations, intensity, and polarization.*
2. *Detailing of detectors and apparatus performance criteria.*
3. *Discussions of background criteria including radiation levels at detectors.*
4. *A run plan including*
 - (a) *milestones and times for achieving 1, 2, and 3.*
 - (b) *count rates and running times to achieve statistical uncertainties.*
 - (c) *auxiliary measurements and times to control systematic uncertainties.*

This document is, therefore, an update that focuses on the issues above. The details of the motivation, the experimental technique and the apparatus are contained in the PAC 28 proposal [1]. Because one of the important issues detailed above is related to performance criteria, we collect in Table 0.1 key criteria from the various sections that follow.

The remainder of this document is organized as follows. The first section outlines both the basic running conditions and technical considerations and recent developments connected with apparatus performance (including shielding and beam polarimetry issues). Section 2 deals with systematic uncertainties including those from helicity-correlated beam properties (see Appendix B for the beam specifications), transverse beam asymmetries and background corrections. The third section presents the ancillary measurements anticipated during the normal running of the experiment. We conclude in Section 4 with a detailed discussion of the uncertainties and the beam time request. For reference, Appendix A contains the updated collaboration response to the TAC questions from PAC 28 and Appendix B contains the beam parameter specifications for the proposed run.

*Technical Advisory Committee

Subsystem	Description	H/D	Criterion
Target	Boiling	H	$(\delta A/A)_{tb} < 430$ ppm
		D	$(\delta A/A)_{tb} < 350$ ppm
	Minimum power	H	460 W
		D	550 W
	Operating range	H	19 ± 1 K
		D	22.5 ± 1 K
Magnet	z position		2 mm
	Minimum current		2440 A
Detectors	CED/FPD Threshold		$< 1/3$ m.i.p. ($> 5\sigma$)
	Anode current		$< 80 \mu\text{A}$
	Cherenkov efficiency		$> 85\%$
	Cherenkov rejection	D	> 2
	Overall dead-time		$< 20\%$
Acquisition			
Beam	Helicity-correlated charge asymmetry		2 ppm
	Helicity-correlated position difference		40 nm
	Helicity-correlated angle difference		4 nr
	Helicity-correlated energy difference		18 eV
	Halo (> 3 mm radius)		$< 1 \times 10^{-6}$ outside

Table 0.1: *Key performance criteria for experiment subsystems. These requirements will be checked in the lead-up to the 687 MeV run including the 10 days commissioning period for that measurement.*

Contents

1	Experimental conditions	1
1.1	G ⁰ apparatus performance criteria	1
1.1.1	Cryostat exit detectors	1
1.1.2	Cherenkov counters	3
1.1.3	Electronics	5
1.1.4	Target	6
1.2	Radiation background	7
1.2.1	Beam halo specification	7
1.2.2	Shielding of the G ⁰ detectors	8
1.3	Polarimetry	12
2	Systematic Error Mitigation	15
2.1	Helicity correlated beam specification	15
2.2	Transverse spin asymmetries	17
2.3	Elastic signal isolation	18
3	Ancillary measurements	22
3.1	Commissioning	22
3.2	Summary of time estimate for ancillary measurements	24
4	Beam time request	25
4.1	Error budget and expected results	25
4.2	Beam time request	26
A	Appendix A: Response to PAC 28 TAC Comments	31
B	Appendix: Beam parameter specifications for the G⁰ experiment (Backward Angle Running)	35

1 Experimental conditions

In this experiment we plan to make measurements of the backward angle parity-violating asymmetries using both hydrogen and deuterium targets. The nominal central angle for the G0 spectrometer in the backward angle configuration is 110° , thus fixing the incident beam energy in order to achieve a desired Q^2 . The experiment will run at $80 \mu\text{A}$ beam intensity and utilize a 20 cm long cryogenic target. For reference, the kinematics, expected (quasi-)elastic rates (full spectrometer acceptance), and nominal asymmetries for $Q^2=0.23 \text{ GeV}^2$ are shown in Table 1.1. The rates are integrated over all the detectors (eight octants).

Target	E (GeV)	E_f (GeV)	θ ($^\circ$)	Q^2 (GeV^2)	Rate (MHz)	Asymmetry (ppm)
^1H	0.360	0.240	110	0.23	4.5	-13
^2H	0.360	0.240	110	0.23	6.8	-18

Table 1.1: *Elastic and quasi-elastic kinematics, rates at $80 \mu\text{A}$, and nominal asymmetries. Those rates takes into account the full acceptance of the G^0 apparatus, that is the eight octants.*

This chapter first describes the detectors and electronic efficiencies of the experiment as well as issues related to the radiation background and the polarimetry.

1.1 G^0 apparatus performance criteria

The detector package for the backward angle measurements has been designed in order to optimize the selection of elastically scattered electrons from other negatively charged particles: inelastically scattered electrons and pions. The models used to evaluate the background rates have been checked against experimental data and are described in the original proposal [1]. Table 1.2 shows the expected rates in each octant broken down by the source of the background. Figure 1.1 shows the distribution of those rates on the CED-FPD matrix. Also shown on this plot are the CED-FPD pairs for which the elastic rates are expected to represent more than 90% of the total yield, these pairs comprise the elastic locus.

1.1.1 Cryostat exit detectors

It is difficult to transport the scintillation light from these long narrow scintillators. However, the final tests on all 72 assembled detectors show good light amplitude (> 50 p.e. for all photo-tubes) and good signal balance on either side of each scintillator. Figure 1.2 shows the light amplitude results from the CED testing.

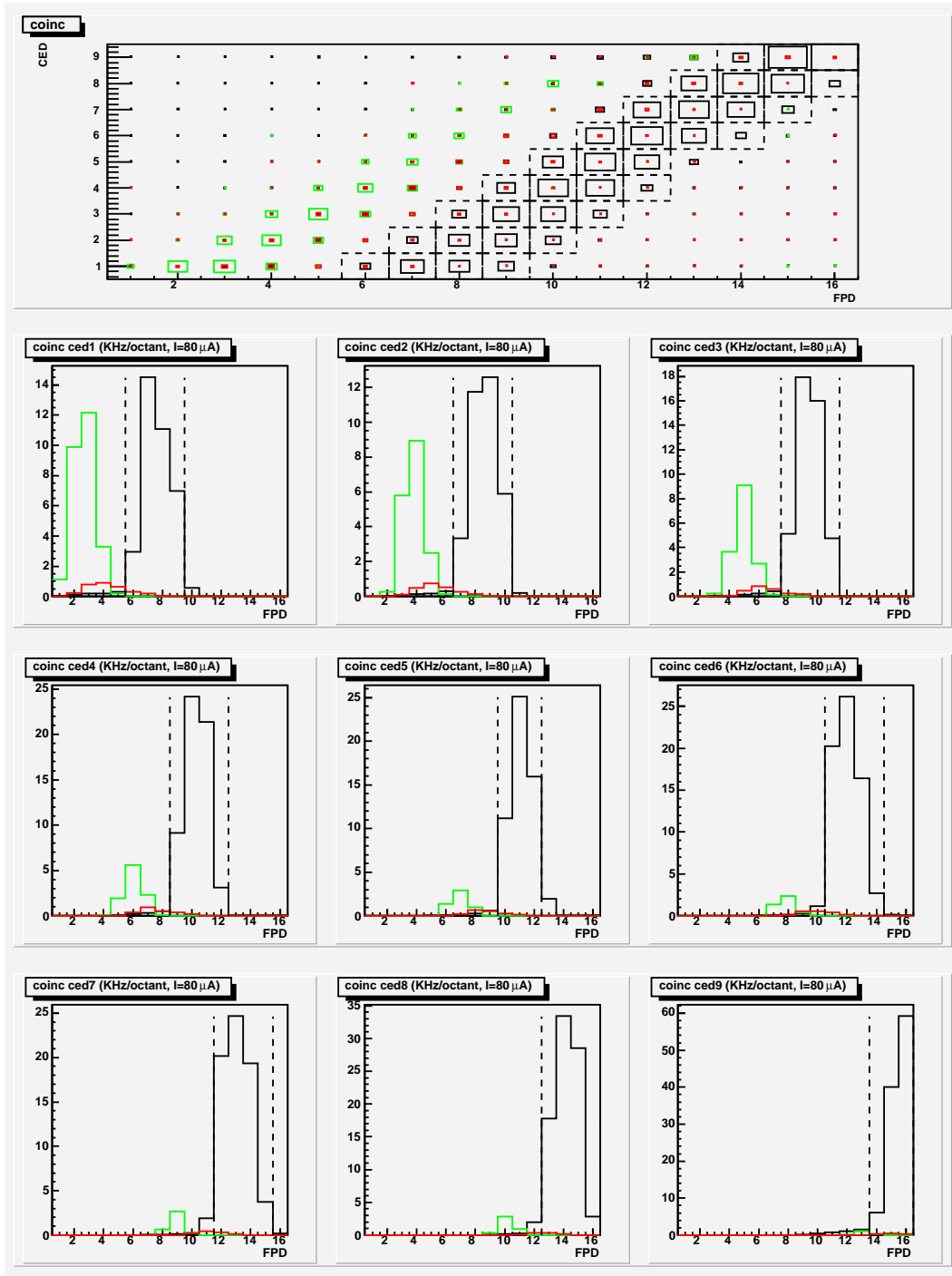


Figure 1.1: Rate distributions for the LH2 measurement $80 \mu\text{A}$. The upper plot shows the rates (in kHz) in the CED versus FPD matrix, the elastic locus appears as a line at roughly 45° . Each lower plot shows the distribution of the rates for each CED as a function of the FPD number. The elastic rates are in black, the inelastic electrons are in green and the pion (before Cherenkov rejection) are in red. On each CED plot, the vertical lines show the elastic locus for which the elastic rates represent at least 90% of the total rates.

$E_{beam}=360$ MeV Target	Rates (kHz)		
	elastic e^-	inelastic e^-	π^-
^1H	564	90	0
^2H	844	29	305
target end cap	-	16	15
total LH2	685		
total LD2	1285		

Table 1.2: *Expected rates in one octant for the 360 MeV measurement off hydrogen and deuterium target with a beam intensity of $80 \mu\text{A}$. The rejection of pion by the Cerenkov detector is not taken into account.*

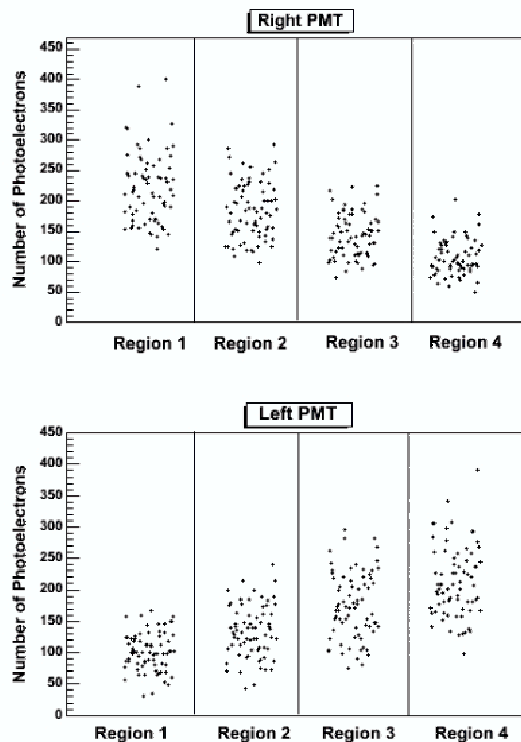


Figure 1.2: *Performance of the CEDs after final assembly. Each CED is divided into four sections azimuthally with Region 1 on the right.*

1.1.2 Cherenkov counters

The G^0 detector package for the backward angle has been supplemented with aerogel ($n = 1.03$) Cherenkov counters to distinguish pions and muons from electrons. The

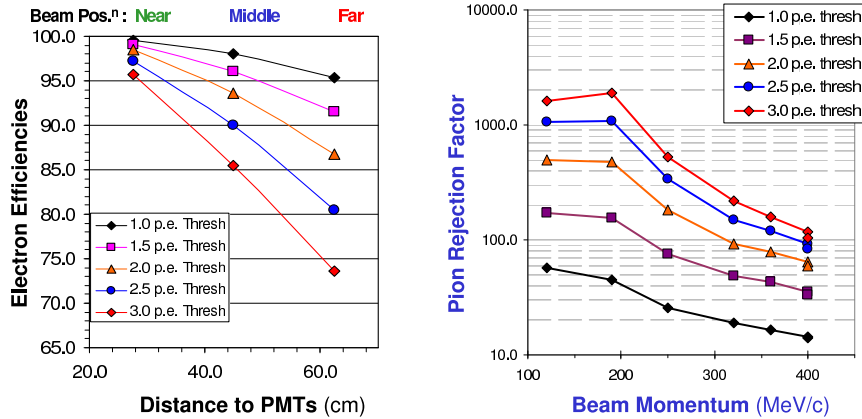


Figure 1.3: *Performance of the Cherenkov counter as tested with the mixed beam at Triumf. In the G^0 configuration a threshold of 2-3 photo-electrons will be used. The right panel shows the electron efficiencies as a function of the hit position in the counter. The right panel shows the pion rejection factor as a function of the momentum of the pions.*

pion(muon) threshold is 560(430) MeV. These detectors were designed to reduce the pion contribution to the total yield to less than 10%. The $(\pi + \mu)/e$ ratios expected within the elastic locus at 0.360 and 0.799 GeV* are shown in Table 1.3. The $(\pi + \mu)/e$ ratio at 0.360 GeV beam is small even for deuterium and the pion rejection ratio of 100 achieved for these detectors (see below) will be more than adequate. A complete description of the Cherenkov counter can be found in the original proposal [1] section 4.1.3 (page 29).

The Cherenkov counter were tested at Triumf using a mixed particle beam of momentum up to 400 MeV/c. The results of the test are shown on figure 1.3. With a threshold of the order of 2-3 photo-electrons, the pion rejection is larger than 100 and the electron efficiencies are (in average) 90%. This is sufficient for the worst case scenario (LD2 target at 0.799 GeV beam energy) and obviously more than enough for the measurements at 0.360 GeV beam energy. We note again that the yield and asymmetry of the pions will be measured simultaneously, allowing offline correction.

E_{beam} (GeV)	$(\pi + \mu)/e$ ratio		p_{π} range MeV/c	p_{μ} range MeV/c
	LH ₂	LD ₂		
0.360	0.002	0.10	100-245	50-225
0.799	0.25	8.4	100-375	50-350

Table 1.3: *$(\pi + \mu)/e$ ratio expected within the elastic locus and kinematic factors for the pions and the muons for the beam energies used to design the Cherenkov counters Here only elastic and quasi-elastic electrons are counted in the denominator.*

*The latter beam energy determined the original design of the Cherenkov counters.

1.1.3 Electronics

The philosophy of the backward-angle electronics design is based in large part on the fact that the electrons being detected ($E_{scattered} \geq 200$ MeV) are all moving with approximately the same velocity, and therefore have a well defined flight time for each CED and each FPD. A negatively charged particle produced in the target will travel through the magnet, the CED array, the Cherenkov counter and the FPD array in sequence. The G0Geant simulation of the experiment has shown that particles detected in a specific FPD are detected within a window of 1 ns by the CED, independent of the CED they go through. This simulation also showed that particles created by a given beam burst will be detected in the FPD array within a window of 3 ns independent of the FPD they are detected in[†]. Therefore, the electronics is triggered in the conventional manner (contrary to the beam trigger scheme used in the forward measurement) by detection of an event by any CED and any FPD and without needing to identify a specific CED-FPD pair.

Figure 1.4 is a simplified representation of the electronics for one octant. Two sets of electronics are used (as in the forward measurement) one French and one North-American which differ in some details [1]. A complete electronics block diagram of the French version can be found in Figure 4.15 of the original proposal. The trigger pulse is generated by an OR of all 14 FPDs ANDed with an OR of all 9 CEDs. The signal from the Cherenkov detector, will be used to enable a latch which allows the coincidence information to be sent to the scaler modules. Additional counting of CED and FPD singles rates, with various combinations of multiple hit logic and Cherenkov signals included, will be used for an estimate of the front end electronics dead-time. Finally, the CED-FPD rates will also be counted in anti-coincidence with the aerogel Cherenkov counter signals in order to measure pion asymmetries. Thus pion backgrounds will not only be suppressed in the Cherenkov coincidence requirement, but will be characterized in detail.

The dead-time of the electronics is important as it couples both to the beam charge asymmetry and the actual measured asymmetries to form a potentially significant false asymmetry. This dead-time can be divided in several parts. The first contribution comes from the dead-time at the trigger level, which is about 32 ns. We also expect significant background ‘singles’ counting rates associated with individual CED and FPD photo-tubes as well as with individual CED and FPD mean-timers. These rates are difficult to estimate. We provide two examples. The elastic rates for deuterium will produce a trigger dead-time of about 2.7% . If we consider background singles rates of 100 kHz/(single mean-timer) and 500 kHz/(single CFD), the overall dead-time increases to 14% . This dead-time is expected to be about the same for different cells of the coincidence matrix if the background counting rates is well distributed over the octant. We expect to be able to measure the dead-times with relative uncertainties of about 10%. Based on that determined for the forward run, the charge asymmetry will be measured with a precision of 0.3% while based on the statistic we will take on the LH2 or LD2 target the physics asymmetry will be measured with a precision of $\sim 2\%$ of its value. Therefore the overall asymmetry uncertainty will be of the order of 0.005 ppm ($\sim 0.14 \times 0.1 \times 0.3$), a negligible contribution to the

[†]These windows of coincidences are even tighter than what was presented in the original proposal. The newest evaluation includes signal travel within the long FPD light guides.

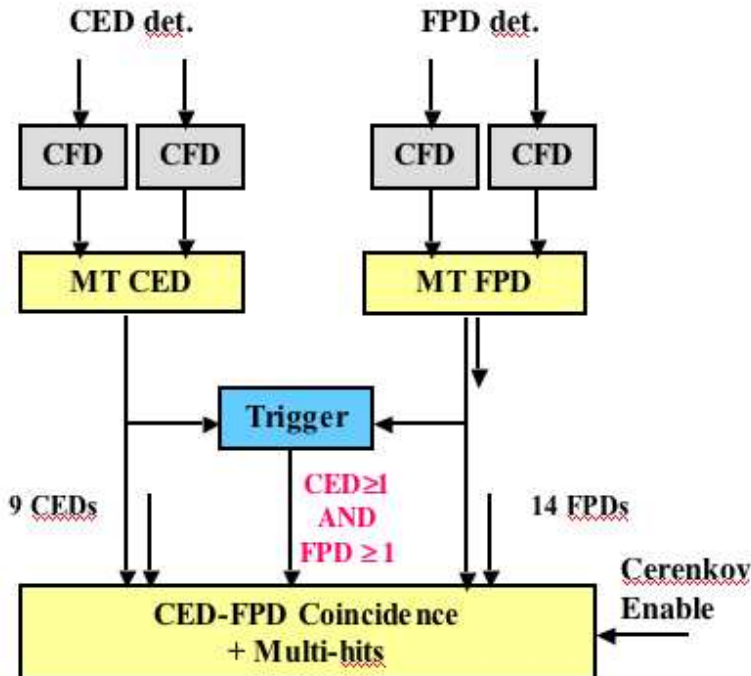


Figure 1.4: *Simplified diagram of the electronics for the backward angle measurements for one octant. The CED-FPD coincidence increments the appropriate scaler depending on the detected CED-FPD pair. There are $14 \times 9 \times 2$ scalers corresponding to all the CED-FPD pairs with and without the Cherenkov signal (electrons and pions, respectively).*

overall uncertainty. Potential triggers with more than one CED or FPD hit will be scaled separately in order to correct for pile-up.

1.1.4 Target

The backward angle running of the G^0 experiment will utilize a slightly modified configuration of the liquid hydrogen target that has been successfully used for the forward angle measurement. The details of this modification can be found in the original proposal [1], Section 4.4 (page 42).

We expect to be able to run the backward angle measurement at $80 \mu\text{A}$, in part because we will be using the standard 499 MHz pulse structure[†] and in part because of the better-than-expected target performance during the forward angle run. This will help us to reduce the overall uncertainties in extracting the form factors whose uncertainties were dominated by the backward angle statistical precision. We have determined from the forward measurement that the total power handling capability will be more than sufficient for this purpose. In addition, we estimate that the contribution of target density fluctuations to the detector asymmetry widths due to the increased power density will be less than 350 ppm even for

[†]The injector would have limited the beam current to just over $40 \mu\text{A}$ with the 31 MHz pulse structure of the forward angle run

an 80 μA beam current, as compared with the minimum statistical width of about 1050 ppm for deuterium [2].

1.2 Radiation background

1.2.1 Beam halo specification

This section discusses in detail the beam halo specification contained in the beam requirements document for the backward angle run provided to the laboratory (see Appendix B). The specification for the beam halo is that it be $< 1 \times 10^{-6}$ of the main beam outside a radius of 3 mm. This is the same as the specification which was met on a routine basis during the forward angle run. It is important to note that this specification was achieved for the 31 MHz time structure beam, which had the potential for more significant halo due to space charge effects in the injector. For the backward angle running we are returning to the normal 499 MHz time structure, so it seems unlikely that the already routinely acceptable halo will get any worse. We also note that the main source of halo is usually thought to be the injector which will operate at its normal ~ 45 MeV energy even for the 360 MeV beam energy.

There are two ways that significant beam halo could potentially be problematic for the experiment. They are interaction of the beam halo with thick parts of the G^0 target flange and interaction of the beam halo with some small upstream aperture.

First we consider interaction of the beam halo with the thick parts of the G^0 target flange – this situation is unchanged from the forward measurement. The beam halo specification above primarily comes from the desire to minimize the interaction of any part of the beam with the thick parts of the target flange which start at a radius of 5.5 mm. During the forward angle run, we monitored this specification by continuously running with an aluminum target (2 mm thick) with a 6 mm diameter hole in it located about 8 meters upstream of the G^0 target. On the outside of the beam-pipe downstream of this “hole” target, there were photomultiplier tubes with scintillator attached. We calibrated the system by putting 5 nA of beam directly into the 2 mm thick part of the aluminum halo target. From this, we could directly show that the above specification was being achieved, and we monitored it continuously during running. The specification was routinely achieved except in some cases where the tune had suddenly ‘gone bad’ due to some significant change in the accelerator or transport line; usually the cause was clear.

The other way beam halo can affect the experiment is through the interaction with some small upstream aperture. The potential problem here is that beam interacting with a small upstream aperture could generate background that is detected in our scintillators. To measure this, we move the main G^0 target and the halo target out of the beam. During the forward angle run, this rate was completely negligible. However, during the forward angle running the scintillation detectors were downstream of the magnet, which provided some protection against backgrounds of this type. In the backward angle mode of running, the detectors are upstream of the magnet, so they do not have this protection.

We can make an upper limit estimate on how big the background from this source might be by looking at some halo monitor rates we have from the forward angle run. The halo monitors consisted of small pieces of scintillator located at the nearly the same z location along the beam-line where the FPD scintillators will be located for the backward angle run. The only difference is that the halo monitor scintillators were located about 10 inches radially from beam centerline, while the nearest FPD scintillator is about 41 inches from beam centerline. To try to extrapolate from the rates measured at 10 inches to the expected rates at 41 inches, we need to guess where the likely origin of these events is. For this estimate, we will assume that they are coming from the smallest aperture in the upstream Hall C beam-line, which is the 2.2 cm inner diameter ceramic beam-pipe through the fast raster magnets. This is 41 meters upstream of where the halo monitor was. Therefore, these detectors saw scattered particles at an angle of about 0.35° , while the nearest FPD has an angle of about 1.45° relative to that location. We have looked at estimates of charged particle production from few GeV electron beams as a function of angle for various processes including Møller scattering, electron-nucleon and electron-nucleus scattering, and electromagnetic showers in few percent radiation length targets. Among these processes, Møller scattering decreases with angle the least rapidly; the rate per unit solid angle falls by a factor of 100 from 0.35° to 1.45° . For our estimate, we assume this drop of a factor of 100. The observed count rate at $40 \mu\text{A}$ for a 2 inch diameter piece of scintillator at 10 inches from the beam centerline was about 20 kHz. Scaling up to the area of the nearest FPD (178 cm^2), to a beam current of $80 \mu\text{A}$, and assuming the factor of 100 drop yields an estimated count rate of 4 kHz. This is smaller than the typical expected 150 kHz count rate in a typical detector. More importantly, it only contributes a 100 Hz increase in the random coincidence rate, which is small compared to the typical 50-100 kHz FPD-CED coincidence rate due to our real signal. This estimate is probably conservative because the threshold on the beam halo monitor was set lower than our expected FPD threshold.

In conclusion, it appears that beam halo should not be a problem for the backward angle run provided the halo is similar to what was routinely achieved during the forward angle run.

1.2.2 Shielding of the G^0 detectors

Shielding for the backward angle measurement was designed with Geant MC simulations, based on Pavel Degtiarenko's version of the code with the G^0 setup and shielding added and calibrated using rates measured during the forward measurement. While the background load is significant, we expect that all detectors can be safely operated with $80 \mu\text{A}$ of beam current after the desired shielding has been installed. The Monte-Carlo predicts that background level at 360 MeV will be similar to or lower than at 687 MeV beam energy. Thus the running conditions established during the early higher energy run should be acceptable for 360 MeV as well.

The code counts events and integrates the energy deposited in the G^0 scintillation detectors. Of special interest here was to determine the limit on the photo-multiplier (PM) tube gain

imposed by the background events (gammas, neutrons, e^- , e^+ , μ^- , μ^+ ...) in the detectors during the experiment. The limits to consider are:

- the PM tube gain has to be small enough that the anode current in the PM tubes does not lead to serious deterioration of the tubes during the experiment (i.e. below about $80 \mu\text{A}$);
- the overall gain needs to be large enough that the signals, above noise, can be reliably detected by our electronics.

To convert the MC energy loss results to anode currents we compared MC results for the backward configuration with those for the forward configuration, scaling the beam current and gain requirement (proton detection for "forward", electron detection for "backward"). The absolute values for PM tube anode currents are estimated to be accurate within a factor of 2.

While gamma and neutron interactions in the detectors only deposit small amounts of energy in the detectors (if they interact, they deposit typically about 25 keV in our 1 cm thick plastic scintillators), their combined detected rates in all 184 detectors are about 10 GHz (with thresholds typically at 10 keV). Charged particles, at combined rates well below 100 MHz, contribute a background load comparable to that of the neutrals due to their much higher energy loss (many of the charged particles are secondaries created outside of the magnet cryostat volume).

To minimize the "avoidable" background the following shielding measures were implemented (see Figure 1.5). Note that many of the details were dictated by limitations in space and overhead crane movement.

- A concrete shielding wall and iron plates enclosing the region leading into the beam dump. The remaining radiation leaking through this shielding contributes only a small fraction to the detector background.
- An aluminum/lead cylinder inserted into the beam pipe enclosing most of the region around the beam between the target and the downstream gate valve. This shield absorbs the large flux of Møller electrons and forward gammas before they interact/scatter from cryostat and magnet elements directly visible by the detectors. The geometry was optimized to avoid the trajectories of the particles of interest and to minimize shower creation from the comparatively rare high-energy scattered electrons.
- Several iron plates and concrete blocks enclosing the area downstream of the cryostat and below the cryostat. These elements were optimized to absorb more radiation (mostly re-scattered from the beam pipe, concrete wall, and the concrete floor) than they create.
- A combination of sheets of Pb, Al, and Polyethylene on the upstream end-cap of the cryostat and around the upstream beam pipe to attenuate as much of the radiation emerging from the cryostat volume as is possible without covering the paths through the exit windows of the particles of interest.

Most of the remaining radiation seen by the detectors originates inside the cryostat volume often by re-scattering from the internal lead collimators and other structures of or within

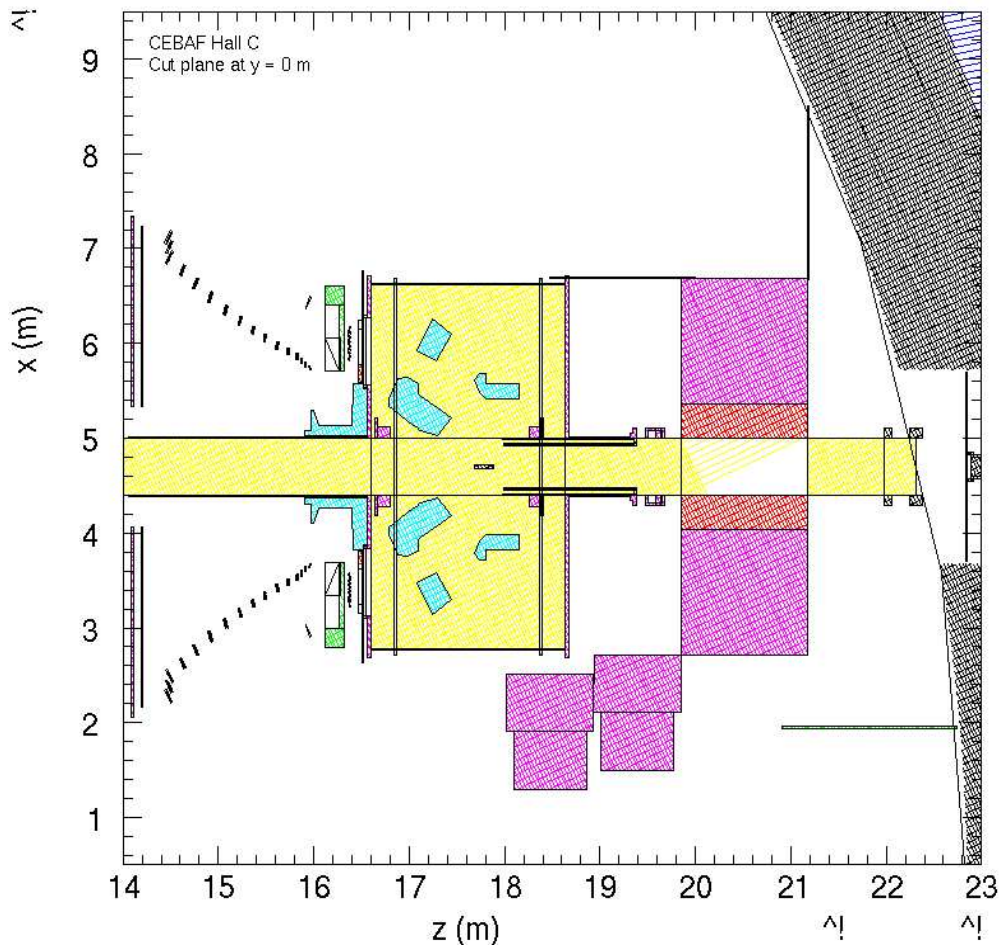


Figure 1.5: *Horizontal cut through the G0 setup with the beam going to the right into the beam dump tunnel visible on the right. On beam left two steel shielding plates touch the concrete shielding wall spanning the beam-line. On beam right a further steel shielding plate and two concrete shielding blocks are visible. The Al/Pb shielding insert is visible upstream of the shielding wall and downstream of the target (center of the cryostat) in the beam-line. Some of the upstream shielding is recognizable: a lead sheet covers most of the visible upstream beam-line and a Pb/Al/Polyethylene sandwich is mounted parallel and upstream of the left cryostat end-cap (between the endcap and the CEDs).*

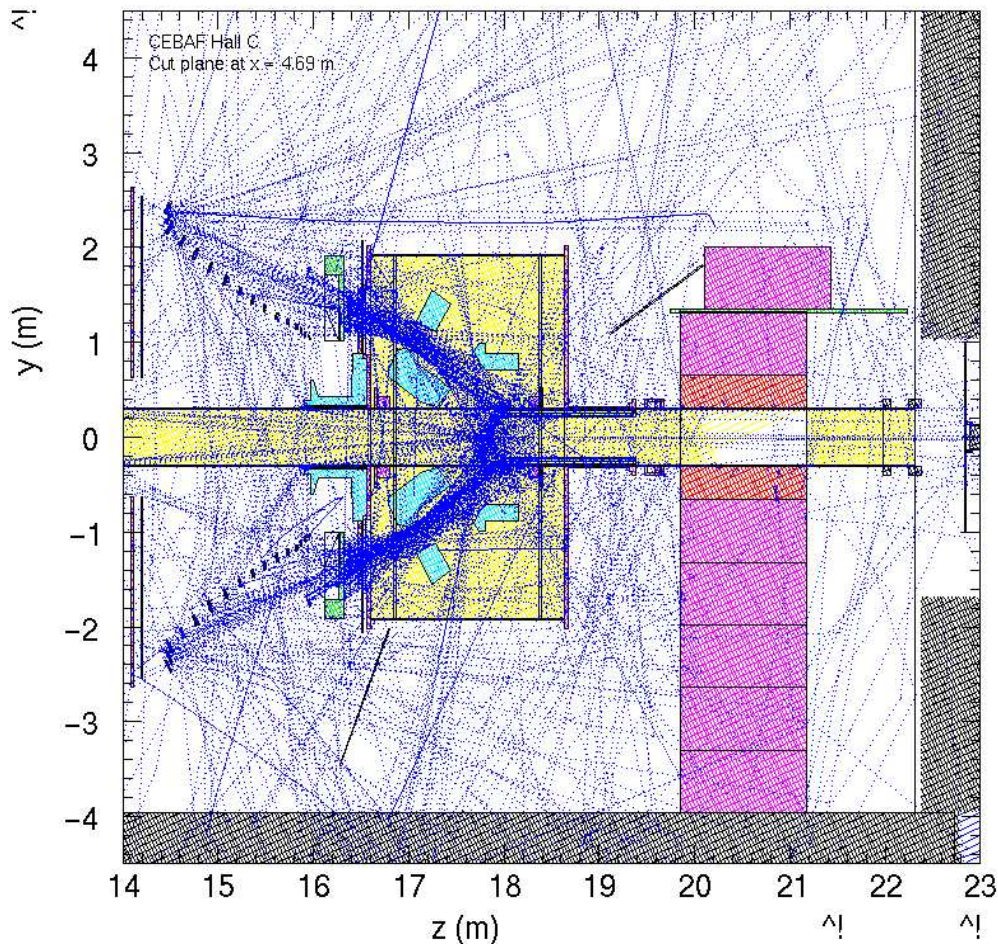


Figure 1.6: *Vertical cut through the G0 setup with traces of gammas hitting the detectors projected on the vertical plane. Traces stop in the detector. The concrete shielding wall with two steel plates near its top is visible between the cryostat and the beam dump tunnel entrance on the right. A tilted steel shielding plate is also visible below the cryostat.*

the cryostat. Figure 1.6 shows a vertical cut through the setup with traces of gammas interacting in a detector.

All detectors are predicted not to exceed the desirable upper limit of $40 \mu\text{A}$ anode current per detector - except for cryostat exit detectors (CED) # 9. CED9s are the largest CED detectors and have the "best" view of the cryostat region near the target. We will reduce the PM gain of CED9s by about a factor of 5 and compensate for the gain loss with additional amplifier modules near the respective PMs. We will have an extra set of amplifiers (e.g. for all CED8's) available in case we find excessive background on additional detectors.

1.3 Polarimetry

The Hall C/Basel Møller Polarimeter was originally designed to operate at beam energies ranging from ≈ 1 GeV to 6 GeV. The low energy limit is essentially given by the aperture presented at the exit of the first of the two quadrupoles. The larger (lab) scattering angle of the Møller electrons results in events that cannot transport successfully to the end of the quadrupole without hitting the beam-pipe or magnet proper. This is illustrated in Fig. 1.7.

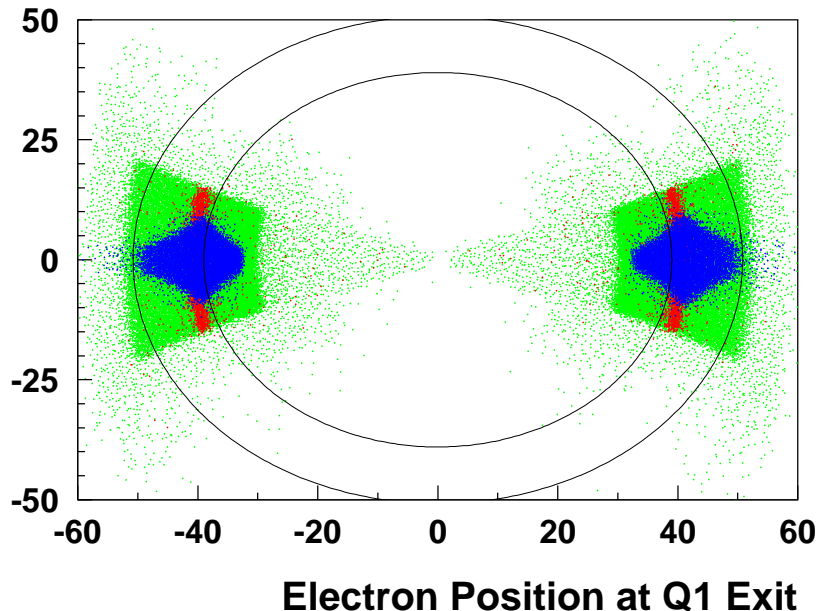


Figure 1.7: *Møller electrons at the exit of the first quadrupole at low energy (in this case, 500 MeV) and with the standard tune. The inner circle represents the beam pipe aperture. Red points are Møller events at 90 degrees (center of mass) while blue points indicate events that would be accepted at the detector plane (ignoring the fact that many of these events would not clear the beam pipe).*

In order to accommodate lower energies, the Møller polarimeter can be reconfigured, moving the first quadrupole closer to the Møller target, allowing the scattered electrons to clear the first quadrupole. This was done first in 2000 for experiment E93-038. In this case, a shift of 6 inches allowed the Møller to be used down to about 800 MeV. For G0 backward angle running, we plan to move the first quadrupole an additional 8.75 inches closer to the Møller target. This shift will allow us to use the Møller in its nominal focusing tune for the higher energy G0 point (687 MeV). At 360 MeV a new tune will be required, which will result in some increase in the systematic uncertainty of the extracted polarization.

Typically, the Møller polarimeter focuses electrons scattered at 90 degrees (in the center of mass) to an ellipse of half-width 49 cm and height 16 cm at the detector plane. Scintillators allow one to measure the correlation between the left and right detectors such that the Møller magnets can be tuned empirically. One of the strengths of the Møller Polarimeter is that this correlation is basically independent of beam energy when the magnets are properly set. At 360 MeV, we will require stronger horizontal focusing in the first quadrupole to successfully pass through all existing apertures. The resulting ellipse at the detector plane has the same size horizontally, but is much larger vertically, a half-height of 70 cm (a comparison of the left–right correlations for the nominal and altered tune is shown in Fig. 1.8). This modification of the Møller optics significantly alters the left–right correlation seen in the Møller detectors and reduces our ability to set the magnets empirically. Because of this, the resulting uncertainty in the measured polarization will be larger. For example, for the G0 forward angle measurement, we estimated that the uncertainty in the extracted polarization (ignoring issues of extrapolation to higher currents) to be about 0.86%. At 360 MeV, Monte Carlo studies indicate that, optimistically, we could achieve a precision of about 2%. It is possible, though, that the precision could be worse, depending on how difficult it turns out to be to set the magnets in this altered tune.

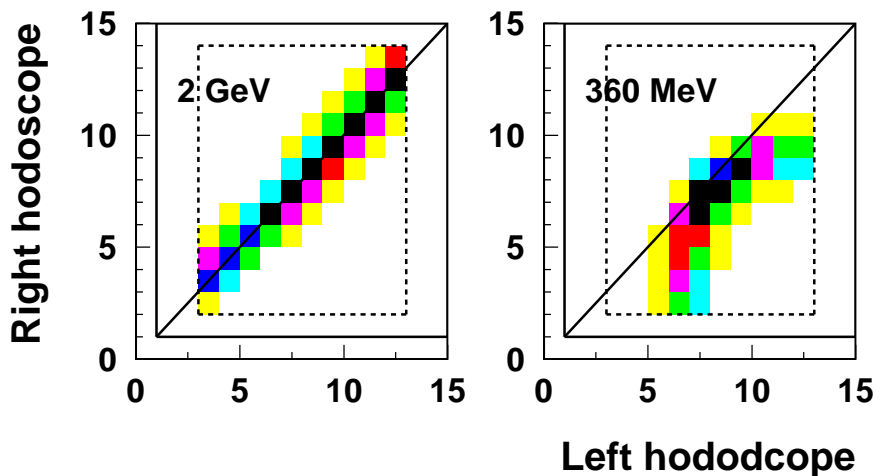


Figure 1.8: *Left–right correlation plots for the nominal Møller magnet tune (left) at 2 GeV, and the altered magnet tune (right) at 360 MeV. With the nominal tune, the left and right scintillator hit patterns should form a diagonal line as shown. If the magnets are mis-set, the hit pattern will shift above or below the diagonal, or the ridge will be too wide. With the altered tune, the correlation is no longer one-to-one, and it becomes more difficult to set the magnets empirically.*

Due to the increased systematic uncertainty of the Møller polarimeter at 360 MeV, we will rely extensively on cross-calibration with the 5 MeV Mott. The systematic error of the Mott polarimeter is estimated to be 1 to 1.5%. Historically, the Hall C Møller has agreed with the Mott at about the 1% level. Given time to perform the appropriate

optimization of the Wien Filter, and allowing the source group the time to null out all vertical components of the electron polarization, we feel confident that we will be able to, in the worst case, transfer the measurement of the absolute polarization from the Mott to the Møller. Even with the altered tune, the relative precision of the Møller is better than 1%, so we conservatively estimate that the final uncertainty of the measurement of the beam polarization to be at worst $\cong 2.1\%$. If we assume a 1% uncertainty due to the fact that Møller measurements are made at $2 \mu\text{A}$ instead of the actual running current (the same assumption we made for the forward angle measurement), the overall uncertainty in the beam polarization is $\Delta P/P \cong 2.4\%$.

2 Systematic Error Mitigation

There are three potentially large sources of experimental systematic errors in the G^0 measurements at backward angle: helicity-correlated beam property changes, transverse spin asymmetries and background contributions to the asymmetries within the elastic locus.

2.1 Helicity correlated beam specification

A complete table of beam requirements for the G^0 backward angle running has been prepared for the laboratory. The document containing the requirements along with definitions of the various quantities and explanatory text can be found in Appendix B. A similar document* was generated for the forward angle run, and it served as a useful basis for development work with the Accelerator Division to deliver beam to the experiment with the required properties. In this section, we discuss in more detail the requirements on helicity-correlated beam properties. For the backward angle running, we have made these requirements a factor of two less stringent generally to maintain the size of the maximum correction relative to the statistical uncertainty; a more detailed discussion follows.

Helicity correlations in beam properties such as position, angle, or intensity can generate a false asymmetry:

$$A_{false} = \sum_{i=1}^N \frac{1}{2Y} \frac{\partial Y}{\partial P_i} \Delta P_i. \quad (2.1)$$

Here, Y is the detector yield, P_i represents beam properties including position, angle, intensity, and energy, and $\Delta P_i = P_i^+ - P_i^-$ is the helicity-correlation in those beam properties. We have made estimates of the sensitivity to variation in beam parameters ($\partial Y/\partial P_i$) using a simple point target model; these results are tabulated in Table 2.1. For the forward angle run, these simple point target estimates agree within 50% with the actual measured sensitivities, so we have confidence that these are a reasonable estimate of the sensitivities expected in the backward angle running. The estimates indicate that the backward angle sensitivities are comparable to or less than the sensitivities of the forward angle run. The smallest expected physics asymmetry for the backward angle running is the -13 ppm for the hydrogen running at 360 MeV. This is larger than the smallest asymmetry from the forward angle running, which was -2 ppm. Since the relative contribution of the false asymmetries is less in the backward angle run, we can tolerate larger helicity-correlated beam variations to achieve the same errors resulting from false asymmetries as the forward angle run. For this reason, we have set the requirements on helicity-correlated beam parameters to be a factor of two less stringent for the backward angle running.

*<http://www.phys.vt.edu/~pitt/g0/g0beamspec.pdf>

	Forward angle	Backward angle
$\frac{1}{Y} \frac{\partial Y}{\partial X}$	1 %/mm	1 %/mm
$\frac{1}{Y} \frac{\partial Y}{\partial \theta}$	-2.5 %/mrad	-0.19 %/mrad
$\frac{E}{Y} \frac{\partial Y}{\partial E}$	-3.6	-2.7

Table 2.1: *Comparison of beam parameter sensitivities for forward and backward angle G^0 running.*

The specific helicity-correlated beam parameter requirements for the backward angle running are tabulated in Table 2.2 along with the requirements and actually achieved values for the forward angle running. The only major difference that is likely to affect achievement of these specifications during the backward angle run is the lower beam energy. This will reduce the “adiabatic damping” that provides suppression of the helicity-correlated position differences. This reduction goes as the ratio of the square root of the beam momentum, so we expect about a factor of three less adiabatic damping in the backward angle run. The actual conditions achieved during the forward angle run for beam position differences were a factor of ten better than our backward angle specification even though the full damping was never achieved during the forward run. The Accelerator Division has continued their efforts to improve the adiabatic damping, especially in the injector region. We should therefore be able to accommodate this loss of a factor of three. Also, the collaboration is working with the polarized source group to reduce position differences by improved setup of the Pockels cell on the laser table using techniques developed by the HAPPEX collaboration. The Accelerator Division is also developing a potentially new method of position feedback using corrector coils in the 5 MeV region that could replace the laser-based piezoelectric feedback that was used during the forward angle running. Taken together, these potential improvements of the techniques demonstrated during the forward angle run should be adequate for the 360 MeV run.

Beam parameter	Forward achieved	Forward spec.	Backward spec.
Charge asymmetry	-0.14 ± 0.32 ppm	1 ppm	2 ppm
x position difference	3 ± 4 nm	20 nm	40 nm
y position difference	4 ± 4 nm	20 nm	40 nm
x angle difference	1 ± 1 nrad	2 nrad	4 nrad
y angle difference	1.5 ± 1 nrad	2 nrad	4 nrad
Fractional energy difference	$(1.0 \pm 0.1) \times 10^{-8}$	2.5×10^{-8}	5.0×10^{-8}

Table 2.2: *Helicity-correlated beam parameters averaged over the entire run period. The columns show the achieved results for the forward angle run, the specifications for the forward angle run, and the specifications for the backward angle run.*

2.2 Transverse spin asymmetries

From the forward angle run, we believe that the electron spin direction in Hall C can be set to be $0^\circ \pm 3^\circ$, if the Wien filter is set to optimize the polarization for Hall C via the standard “mini-spin dance”. While a small offset in the beam spin angle has little effect on the magnitude of longitudinal polarization, it can introduce a significant transverse polarization (BNSSA).

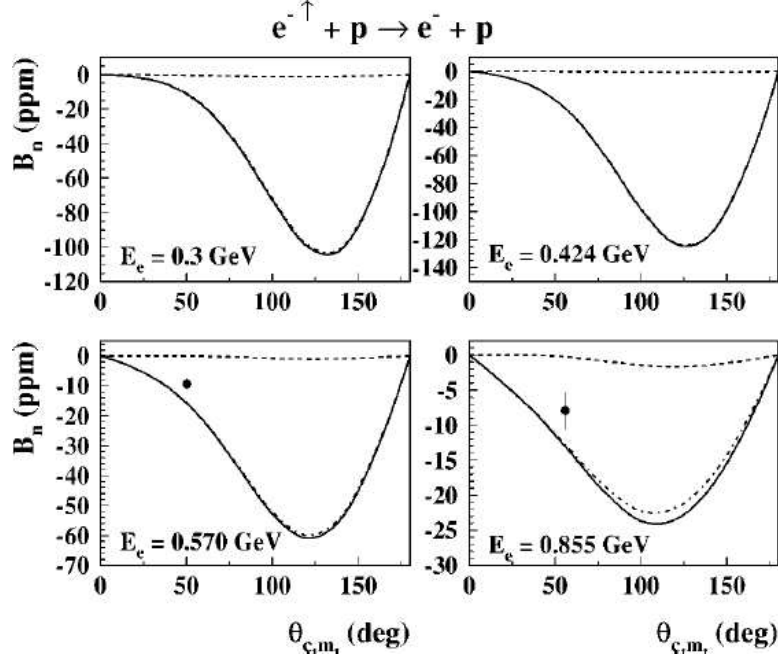


Figure 2.1: *Beam normal single spin asymmetry (BNSSA), B_n calculated [3] in the center of mass scattering angle for beam energies 300, 424, 570, and 855 MeV where the elastic intermediate state contributions (dashed curve) and π - N intermediate state contributions (dashed-dotted curves) are shown as well as the total (solid curve). The data points are from the MAMI A4 Collaboration [4].*

Figure 2.2, taken from Ref. [3], indicates that at a beam energies of 0.3 and 0.424 GeV, the resonance region calculation predicts a beam normal single spin asymmetry of about 100 ppm at the central scattering angle of 130° , so the beam normal single spin asymmetry may be of order 100 ppm at our beam energy of 360 MeV. With a 3° misalignment of the beam spin direction, we would get an azimuthally dependent contribution to our measured asymmetry of about 5% of B_n

$$\begin{aligned}
 A_{meas}^{\parallel} &= P_{\parallel} \cos(3^\circ) A_{PV} + P_{\parallel} \sin(3^\circ) \sin(\phi_{Det} - \phi_{Spin}) B_n \\
 &= P_{\parallel} 0.9986 A_{PV} + P_{\parallel} 0.0523 \sin(\phi_{Det} - \phi_{Spin}) B_n
 \end{aligned}
 \tag{2.2}$$

Therefore we could have a 5 ppm azimuthal variation on our ~ -15 ppm parity violating asymmetry. While we expect that detector averaging should be good to about 2% as it was in the forward measurement, allowing us to largely ignore the azimuthal effects if the

theoretical calculations are correct, a direct measurement of the beam normal signal spin asymmetry would allow us both to verify the scale of the effect and to separate the BNSSA from other effects which may affect the azimuthal variation of the measured asymmetries.

With the beam polarization oriented perpendicularly to the momentum, either in the horizontal or vertical plane, the error on the extraction of the BNSSA is 0.5 times the error on one octant. For the normal running conditions on hydrogen, the elastic rate in one octant is about 500 kHz, leading to an error on B_n in one hour of running of 16 ppm (assuming 75% polarization). In 18 beam hours (one full day of beam time counting the setup times), we should be able to measure B_n in the elastic region to about 3.5 ppm.

2.3 Elastic signal isolation

The presence of background within the elastic locus is a potential source of systematic uncertainties. The measured asymmetry (A_{meas}) in each CED-FPD cell is a mixture of elastic asymmetry (A_{el}) and background asymmetry (A_{back}) depending upon the amount of background present in this cell (dilution factor $f = \text{yield of background} / \text{total yield}$):

$$A_{meas} = (1 - f) A_{el} + f A_{back} \quad (2.3)$$

The method that can be used to extract the elastic asymmetry (A_{el}) is quite similar to the method used for the forward angle analysis. For a given CED, one considers the data provided by all the FPD cells (and vice-versa). One can then model both the yield and asymmetries of the background based on the ranges fixed by their magnitudes and slopes outside the elastic locus. To extract the elastic asymmetry, one then fits the measured asymmetry

$$A_{meas}(FPD) = (1 - f(FPD)) A_{el} + f(FPD) A_{back}(FPD) \quad (2.4)$$

For this method, one assumes to start that the elastic *asymmetry* is constant over the elastic locus, which is realistic as the Q^2 varies very slowly within the acceptance of the apparatus[†]. The extracted elastic asymmetries for each CED are then averaged accordingly to their individual precision to obtain the final results.

This model can be used to estimate the systematic precision of the background correction. We begin with the G0Geant simulation of the background within each CED/FPD cell, including the elastic contribution, the contribution of inelastically scattered electrons and pions from both the target fluid and aluminum target end caps. The dilution factor within the elastic locus is $\sim 3\%$. Figure 2.2 gives an example of these simulated yields as well as an example of the simple model used for the subsequent steps in this estimation (“perfect” yield). To determine the precision of the extraction, we use a simulation. For each ‘run’

[†]The overall acceptance is about $\pm 10\%$ in Q^2 , therefore, the elastic asymmetry varies by a comparable amount over the full acceptance.

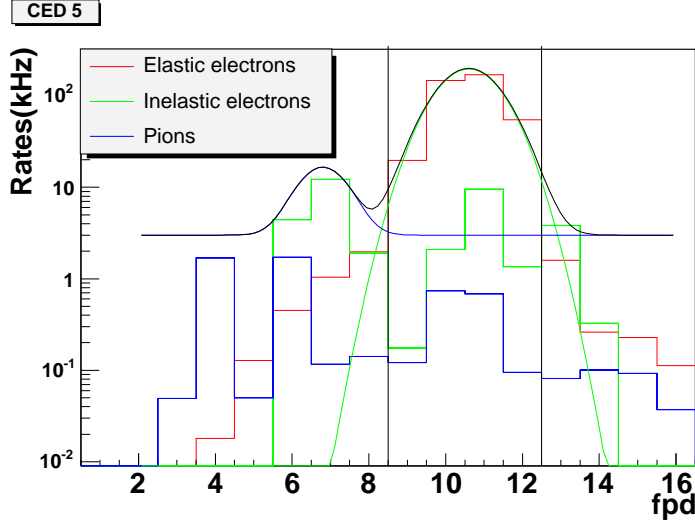


Figure 2.2: Rate distribution for the LH2 measurement at $80 \mu A$ for CED 5 as a function of the FPD number. The vertical lines show the elastic locus. The vertical scale of the plot is logarithmic. The other lines show the functions used to provide a simple model of the yields (elastic, background, and total).

of the simulation, we compose an effective yield distribution using the “perfect” yield model, but allowing the background yield to deviate from this model up to $S\%$ of its value within the elastic locus. For each run, we use an arbitrary, smooth distribution of the background asymmetry. This distribution contains two nodes between FPD 1 and 16 and is defined such that for all FPDs the background asymmetry is contained within a range A_B^{min} and A_B^{max} . Using this smooth background asymmetry distribution, the effective yield distribution, and the given elastic asymmetry (A_{el}^i), one can construct effective asymmetry distribution. The precision of each effective asymmetries depend on the yield used and an arbitrary duration of the faked data. This effective asymmetry distribution is then fit using the “perfect” yield model for the dilution factors, a linear function for the background asymmetry and a constant for the elastic asymmetry. An example of those fits is shown in Figure 2.3. The extracted elastic asymmetry (A_{el}^e) is then compared to the input elastic asymmetry (A_{el}^i) in a large number of runs. The distribution of $A_{el}^e - A_{el}^i$ is a Gaussian whose width is a combination of the statistical precision of the fake experiment and the systematic precision of the extraction. The results of the simulation are given in Table 2.3. We conservatively estimate that the systematic precision arising from the extraction of the elastic asymmetry will to be 1.5% .

Also, as described in the PAC28 proposal, a pair of drift chambers from the HKS experiment will be placed into one octant of the detector system to provide a high resolution position and angle measurement of particles identified in the standard CED-FPD system. This measurement will help to extract dilution factors for the elastic yield. Monte Carlo simulation of the chambers was performed using the $200 \mu m$ resolution measured in the HKS experiment. An example of the simulation with liquid deuterium target and 360 MeV beam energy is shown for FPDs coincident with CED 3 containing significant elastic

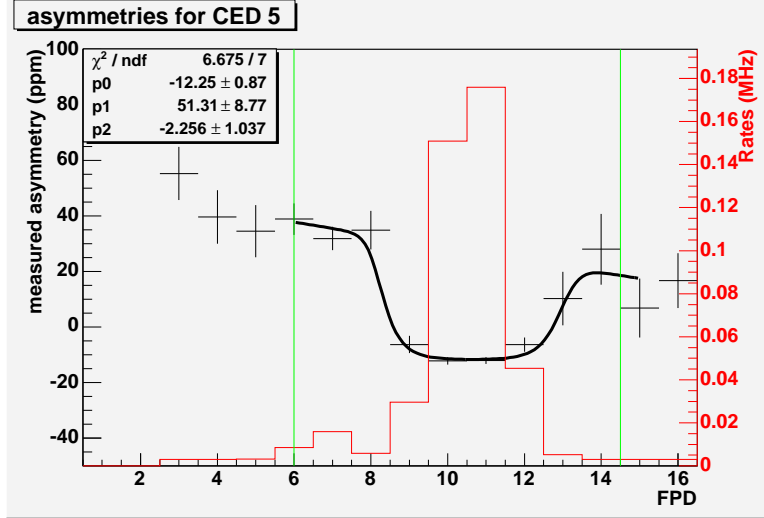


Figure 2.3: *Example of the fits used to extract the elastic asymmetry from the asymmetry measurements. The data correspond to one specific CED only. For this particular example, the background asymmetry is allowed to vary between +40 ppm and 0 ppm.*

dilution factor (%)	Background yield error (S in %)	A_B^{min}, A_B^{max} (ppm)	$\Delta A_{sys}/A_{PV}$ (%)
3	50	-23,-3	0.89
3	50	-33,+7	0.95
3	100	-33,+7	1.02
9	50	-23,-3	1.31
9	50	-33,+7	1.65

Table 2.3: *Relative systematic errors due to the extraction of the elastic asymmetry from the measured asymmetry using the simulation described in the text. Within the elastic locus the background rates represent $\sim 3\%$, the computation was also performed for a dilution factor of 9%. The knowledge of the dilution factor and the minimal and maximal value of the background asymmetries are also varied around the actual PV asymmetry of -13 ppm in the hydrogen case.*

signal (Fig. 2.4). Inelastic electron yield is included in the simulation but accounts for $< 1\%$ of the electron yield (Fig. 2.5). A smooth background at the level of 10% of the elastic was generated with an exponential function and added to the elastic and inelastic electron yield. Fitting this combination with a Gaussian for the signal and second order polynomial for the background yielded an estimate for the dilution factor uncertainty of 3%. Estimations of the *chamber current* from all background in the hall based on recent Monte Carlo indicated that a beam current of less than $10 \mu\text{A}$ will be necessary to stay below the $200 \mu\text{A}$ threshold of the high voltage supply.

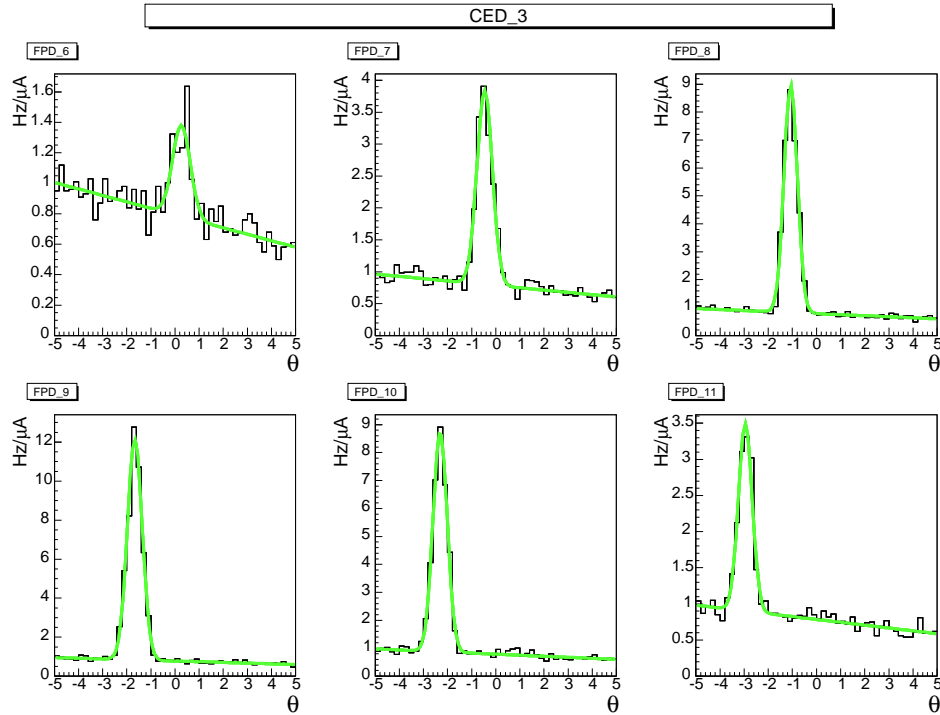


Figure 2.4: Results of 360 MeV, liquid deuterium Monte Carlo for electrons coincident with CED 3 and FPDs containing significant elastic yield. A 10% exponential background is added. Fits with Gaussian plus Polynomial give an estimated 3% error in extracted dilution factors.

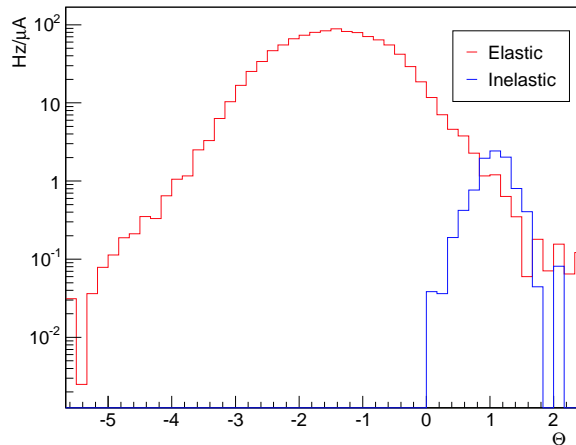


Figure 2.5: Complete elastic and inelastic electron rate seen by drift chambers at 360MeV from a Liquid deuterium target. The inelastic contribution is < 1% of the total. This is reduced further still with a hydrogen target.

3 Ancillary measurements

This chapter first describes the plan for the backward angle commissioning including check-out of the new detectors and establishing the required performance of each of the subsystems. In the second section, we discuss the routine test measurements to be included in the normal running.

3.1 Commissioning

All systems will be checked out to the extent possible in advance of the approved commissioning time for the 687 MeV run (10 days). These activities include full operation of the magnet and target (with both hydrogen and deuterium and measuring the maximum power handling capacity) and ‘chain test’ checkout of the detectors, electronics and acquisition software using cosmic rays. The chain tests will extend in particular the present understanding, based on individual testing, of the operational characteristics of the new detectors. These tests will also include measurements to characterize the effect of the magnetic field from the SMS on the CED and Cherenkov detector photo-tubes.

Most of the ‘live’ checkout of the experiment will occur during the Mar. 2006 commissioning period preceding the high Q^2 measurement. Based on the forward angle commissioning, we provide in Table 3.1 time estimates for the backward angle commissioning tasks. The goal of this program is to establish the operating mode of the experiment considering simple functionality through to control of systematic effects. This Table also indicates measurements that need to be repeated when lowering the beam from 687 to 360 MeV. A short description of these tasks follows.

- Target

Much of the target commissioning time will be spent investigating the effects of target boiling. Measurements of the asymmetry widths of both the luminosity monitor and spectrometer detector signals will be made while varying raster size, fan speed and beam intensity. The contribution of the target cell endcaps will also be measured.

- Scintillators CED-FPD

Based on the collaboration experience during the forward angle measurements, a total of one shift (8 h) is necessary to adjust the gain of all the detectors using the monitoring electronics. These measurements are made at low beam intensity (a few μA). The next step is to check the anode current of the PMTs at nominal beam intensity (80 μA). If the anode currents are larger than about 40 μA *, additional

*The larger the anode current, the faster the PMTs age and loose gain. During the forward measurement, all PMTs were drawing of the order of 40 μA , and the gain loss was $\sim 10\%$ over the 4 months of data taking.

Task	Initial commissioning $E_{beam}=687$ MeV (h)	Repeat at $E_{beam}=360$ MeV (h)
Target	16	4
Scintillator gain adjustment	8	-
Anode current check and shielding	48	-
Cherenkov	16	-
Electronic checkout	16	4
Beam-line checkout	24	-
Helicity feedback checkout	24	-
Møller commissioning	8	16
Mini-spin dance	8	8
Reverse polarity	24	8
Transverse spin measurement	46	46
Total	9.9 days	3.6 day

Table 3.1: *Time estimates for the commissioning tasks at both 687 (already approved for 10 days commissioning) and 360 MeV.*

shielding might be needed. This last step might be lengthy, but according to our simulation does not need to be repeated when going from the 687 to 360 MeV.

- Cherenkov counter

During the scheduled commissioning in March, our plans include: (a) Studying the background rates and anode currents in the Cherenkov PMTs and adding shielding where/if necessary, (b) “Fine-tuning” the detectors’ response to electrons versus pions; (c) Optimizing the electron triggering efficiency versus the pion rejection factor via modification of the trigger configuration; and (d) Optimizing the relative timing between the Cherenkov detectors and the CEDs.

The integrated beam time required is estimated to be 16 h. When we go from the large Q^2 to the smaller Q^2 , we do not foresee doing anything special to the Cherenkov detector. Since the magnetic field will be lower, we could consider adjusting the PMT positions relative to their magnetic shields (i.e. moving them closer to the Cherenkov box proper), to increase the electron efficiencies. Quantitatively, however, it probably won’t be a very significant effect (the in-situ magnetic field studies, mentioned above, will give us a better estimate of any potential gains).

- Møller & Mini-Spin dance

For normal operation, we generally require about 8 h (1 shift) to commission the Moller Polarimeter at a particular beam energy. In light of the altered tune required at 360 MeV, we conservatively allocate two shifts to cover the magnet setup and polarimeter commissioning. The extra shift will be spent checking systematic effects such as beam position and angle variations, magnet changes, and rate dependences. We will also be checking the relative stability of the polarimeter, as it may not be the same with the modified tune. Finally a shift will be used to perform a mini-spin

dance. In this procedure, the launch angle of the electron spin in the injector is varied using different settings of the Wien filter. For each Wien filter setting, all components of beam polarization are measured using the Mott polarimeter in the injector, and, at the same time, the longitudinal polarization component is measured using the Møller polarimeter in Hall C. The mini-spin dance provides both the cross calibration of the two polarimeters and the optimized settings for longitudinal polarization at the G0 target.

- Electronics

The coincidence electronics will be commissioned during the 687 MeV setup. While a “chain test” will have been successfully completed using pulser signals from the splitters through the coincidence electronics into the scalers and data acquisition, the majority of the commissioning work will be in timing all of the CED, FPD, and Cherenkov signals together with real charged particles scattered from the target through the scintillators and aerogel. We will also calibrate the dead-time corrections based on both yield measurements at different beam intensities as well as asymmetry measurement with large induced charge asymmetries.

- Transverse asymmetry measurement

As described in section 2.2, we plan to perform measurement with the beam polarization oriented in the transverse directions. For each of the target materials (H_2 and D_2), the goal is to take 18h of data. In addition to the liquid targets, we will also run 2 h on the aluminum background target to allow cell wall subtraction. Including injector setup, this measurement will take 46 h.

3.2 Summary of time estimate for ancillary measurements

During the data taking, regular calibrations (beam polarization measurement, helicity correlated feedback calibration, beam current monitor calibration,...) will take place. Based on our experience in the forward angle measurement we provide in Table 3.2 an estimate of the required time.

Activity	Frequency (1/d)	Time/meas (h)	Total (d)
Beam polarization	1/3	4	3.3
Beam energy	1/14	4	0.7
Beam current	1/14	2	0.4
“Coil pulsing”	15	0.01	0.4
Total			4.8

Table 3.2: *Breakdown of estimated times for auxiliary measurements.*

4 Beam time request

4.1 Error budget and expected results

This section presents the error budget and expected results from the combination of the hydrogen forward and hydrogen and deuterium backward angle running at $Q^2 = 0.23 \text{ GeV}^2$. The three measurements ($A_{f,b,d}$ for the forward hydrogen, backward hydrogen, and backward deuterium asymmetries, respectively) are related to the form factors of interest through the relation:

$$\begin{pmatrix} A_f \\ A_b \\ A_d \end{pmatrix} = \mathbf{A} \begin{pmatrix} G_E^s \\ G_M^s \\ G_A^e(T=1) \end{pmatrix} + \mathbf{B} \quad (4.1)$$

where \mathbf{A} and \mathbf{B} are 3x3 and 3x1 matrices, respectively. The elements of \mathbf{A} and \mathbf{B} are functions of electromagnetic form factors and kinematic variables. The explicit evaluation of this expression for $Q^2 = 0.23 \text{ GeV}^2$ is given by:

$$\begin{pmatrix} A_f \\ A_b \\ A_d \end{pmatrix} = \begin{pmatrix} 23.96 & 4.42 & 0.23 \\ 9.76 & 9.46 & 2.83 \\ 7.92 & 2.22 & 3.55 \end{pmatrix} \begin{pmatrix} G_E^s \\ G_M^s \\ G_A^e(T=1) \end{pmatrix} + \begin{pmatrix} -5.01 \\ -11.28 \\ -15.90 \end{pmatrix} \quad (4.2)$$

where the numerical values are in parts per million (ppm). To obtain the desired form factors, the system Eqn. 4.1 is inverted. The errors on the form factors come from the equation:

$$\sigma_{G_X}^2 = \left(\frac{1}{2}\right) \sum_{i=1}^n \sum_{j=1}^n \left[\left(\frac{\partial G_X}{\partial Y_i}\right)^2 \sigma_{Y_i}^2 + \left(\frac{\partial G_X}{\partial Y_i}\right) \left(\frac{\partial G_X}{\partial Y_j}\right) \sigma_{Y_i Y_j}^2 \right] \quad (4.3)$$

where G_X is one of the three form factors of interest ($G_E^s, G_M^s, G_A^e(T=1)$). The σ_{Y_i} are the statistical and systematic errors on the asymmetries, the uncertainties in the electromagnetic form factors, and the uncertainties in the beam polarization (P_e) and squared 4-momentum transfer (Q^2). The $\sigma_{Y_i Y_j}$ are the correlation coefficients between the independent variables Y_i . In our case, the only significant non-zero correlations are for the polarization and Q^2 measurements. The beam polarization error is dominated by systematic errors that will be common to the hydrogen and deuterium measurements. Similarly, the Q^2 measurement relies on the same magnetic field calibration for both hydrogen and deuterium. For both variables, we treat the errors as 100% correlated between hydrogen and deuterium; this results in the most conservative error estimate.

The error on the forward angle asymmetry data is obtained by combining data from the published forward angle experiment that covers the same $\pm 12\%$ range about the nominal Q^2 (0.23 GeV^2) as the backward angle data. That results in a total fractional error (including

the statistical and experimental systematic errors) of 9.3%. The errors on the backward angle hydrogen and deuterium data are tabulated in Table 4.1. These errors assume 30 days of running time each for hydrogen and deuterium and 75% beam polarization. The uncertainties assumed on the electromagnetic and isoscalar axial form factors, beam polarization, and Q^2 measurement are tabulated in Table 4.2.

Source	$\delta A_{PV}/A_{PV}$	
	LH2	LD2
Backgrounds	1.5%	1.5%
Transverse asymmetry	0.5 %	0.4 %
Dead-time	0.3%	0.2%
Total systematic error	1.6 %	1.6%
Beam time	30 days	30 days
Total Statistic Error	3.0 %	1.7 %
Total Experimental Uncertainty	3.4 %	2.3 %

Table 4.1: *Error budget for uncorrelated errors for the proposed measurement at $Q^2 = 0.23 \text{ GeV}^2$ on both the hydrogen and deuterium target.*

To determine the optimum split of running time between hydrogen and deuterium in the backward angle mode, the estimated error on the form factors as a function of the fraction of running time on hydrogen are displayed in Figure 4.1. A broad minimum in the errors on G_E^s and G_M^s is observed in the range 0.4 to 0.7. For simplicity, we choose an even split in the running time between hydrogen and deuterium. The resulting errors on the form factors for that choice are tabulated in Table 4.3 and displayed in Figures 4.2 and 4.3.

Quantity	Uncertainty
$\Delta G_E^p/G_E^p$	1.25%
$\Delta G_M^p/G_M^p$	1%
$\Delta G_E^n/G_E^n$	7.5%
$\Delta G_M^n/G_M^n$	1%
$\Delta P_e/P_e$	2.4%
$\Delta Q^2/Q^2$	1%
$\Delta G_A^e(T=0)$	0.11
ΔR_V^p	0.033
ΔR_V^n	0.0004

Table 4.2: *Uncertainties assumed in the extraction of errors on the separated form factors G_E^s , G_M^s , and G_A^e .*

4.2 Beam time request

We request a total of 68.4 days for the measurement of backward angle asymmetries on hydrogen and deuterium targets including a brief commissioning period as well as time for

Quantity	G_E^s	G_M^s	$G_A^e(T = 1)$
$A_{f,tot}$	0.022	0.010	0.043
$A_{b,stat}$	0.010	0.055	0.012
$A_{b,syst}$	0.005	0.030	0.006
$A_{d,stat}$	0.006	0.035	0.099
$A_{d,syst}$	0.005	0.032	0.091
G_E^p	0.003	0.000	0.020
G_M^p	0.002	0.006	0.006
G_E^n	0.004	0.003	0.009
G_M^n	0.001	0.005	0.016
Q^2	0.008	0.048	0.074
P_e	0.016	0.093	0.146
<i>others</i>	0.004	0.024	0.012
Total	0.032	0.134	0.219

Table 4.3: Contributions to the error on G_E^s , G_M^s , and $G_A^e(T = 1)$ at $Q^2 = 0.23 \text{ GeV}^2$ assuming an even split of running time between hydrogen and deuterium. The entries for Q^2 and P_e include the errors for both the back-angle proton and deuterium measurements added linearly, under the assumption that those errors are 100% correlated. The “others” entry includes $G_A^e(T = 0)$, R_V^p , R_V^n errors added in quadrature.

ancillary measurements during the main data-taking. The breakdown of the time is shown in Table 4.4.

Activity	Time (d)
Commissioning	3.6
Hydrogen	30
Deuterium	30
Ancillary measurements	4.8
Total	68.4

Table 4.4: Beam time request for $Q^2 = 0.23 \text{ GeV}^2$ (360 MeV) measurement.

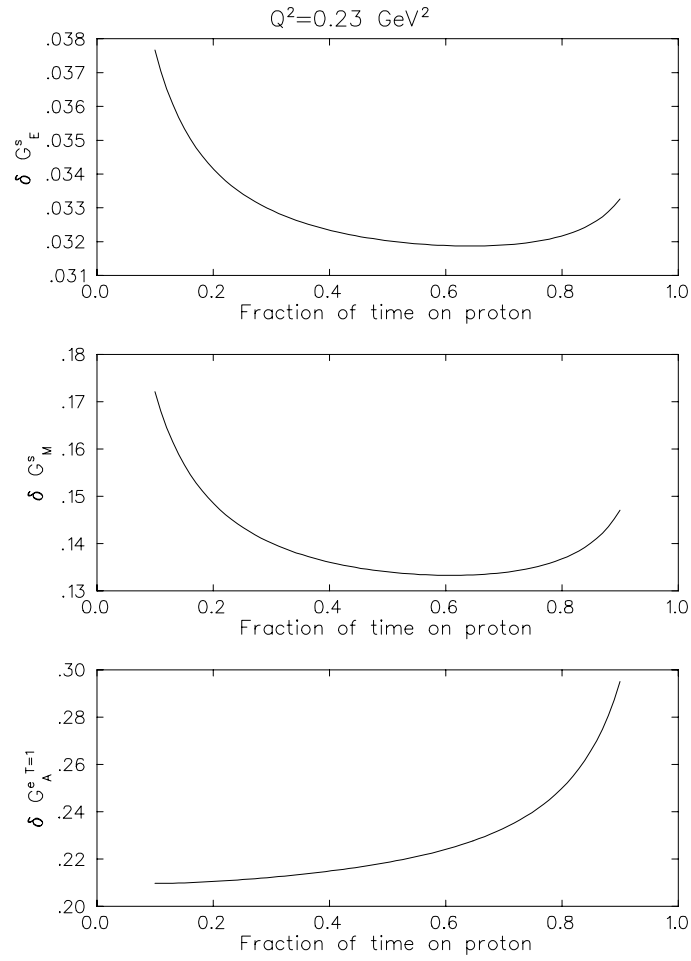


Figure 4.1: Total errors on the separated form factors at $Q^2 = 0.23 \text{ GeV}^2$ as a function of the fraction of the backward angle running time on hydrogen.

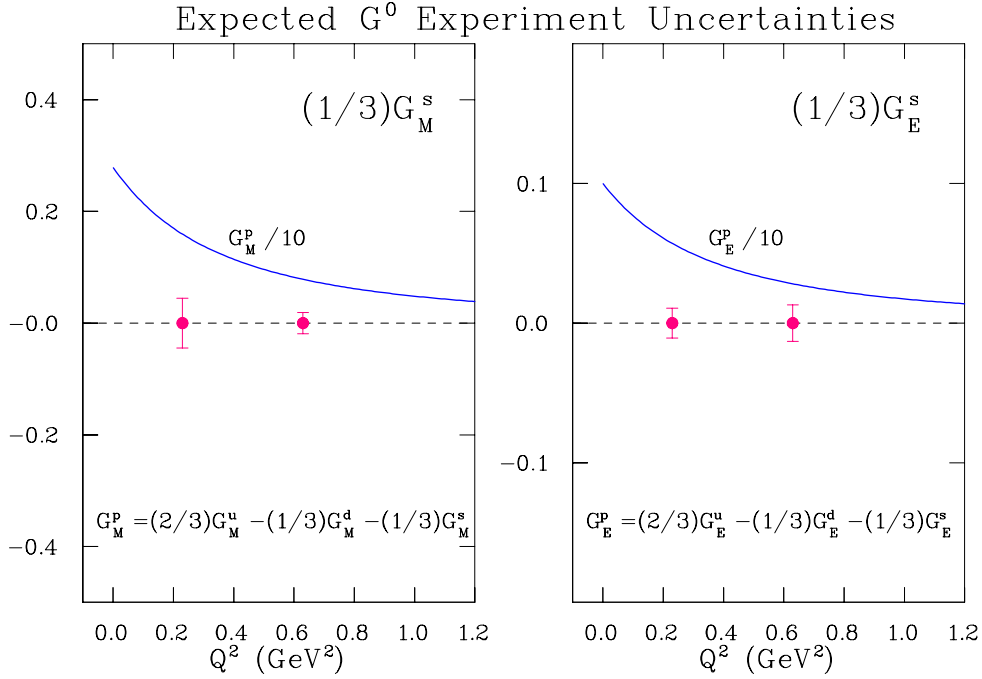


Figure 4.2: *Expected errors on the contribution of the strange form factors to the electric and magnetic proton form factors are shown for the approved point at $Q^2 = 0.63 \text{ GeV}^2$ and this proposed point at $Q^2 = 0.23 \text{ GeV}^2$.*

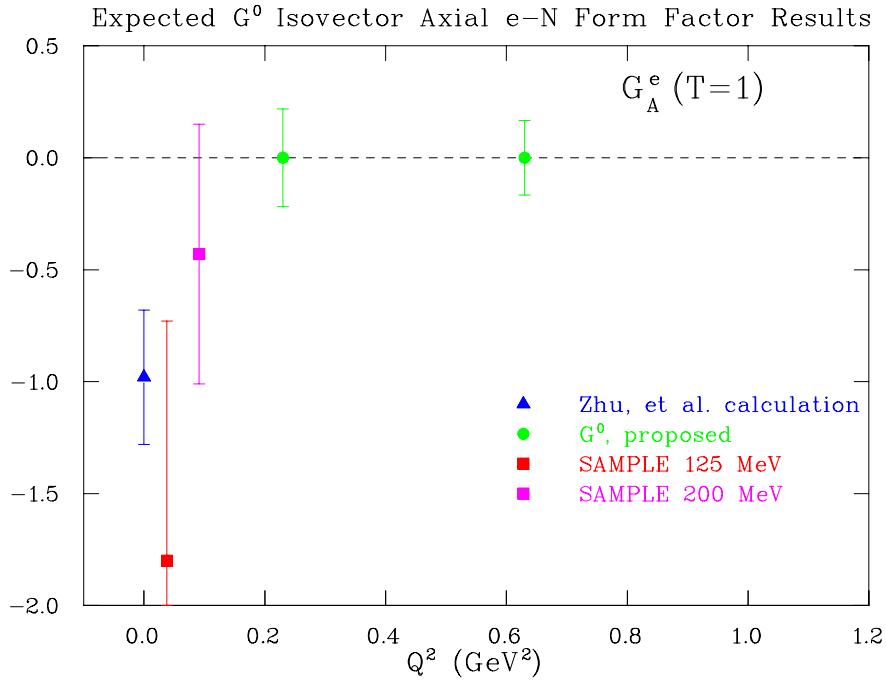


Figure 4.3: *Expected errors on the isovector axial e-N form factor are shown for the approved point at $Q^2 = 0.63 \text{ GeV}^2$ and this proposed point at $Q^2 = 0.23 \text{ GeV}^2$.*

References

- [1] The G^0 collaboration (Spokeperson : D. Beck), *PR 05-108 :The G^0 Experiment Backward Angle Measurements Update.* , presented to JLab PAC28.
- [2] S. Covrig, et al., Nucl. Instr. Meth. A **550**, 218, 2005.
- [3] B. Pasquini & M. Vanderhaeghen, Phys. Rev. **C70**, 045206, (2004).
- [4] F. E. Maas [A4 Collaboration], Prog. Part. Nucl. Phys. **55**, 320, (2005).

A Appendix A: Response to PAC 28 TAC Comments

In this Appendix, we provide answers to questions from the TAC in advance of PAC28.

1. *This is a large installation experiment requiring the G0 apparatus in backward angle mode. Switching from standard Hall C running to G0 is estimated to take about two months and restoration of the standard configuration after G0 running one month, assuming that this is not the first time the G0 backward configuration will be used.*

The backward angle installation is now well underway. The magnet and detector system were turned around in Summer 2004. At the time of writing, they are on the beamline and the new detectors (CEDs and Cherenkovs) have been installed and aligned. Final checks of the target system are being made in preparation for its installation in the magnet scheduled, for early December. We propose to make the low Q^2 measurement in periods contiguous with the $Q^2 = 0.63 \text{ GeV}^2$ measurement to take advantage of this installation.

2. *The beam time request only includes production running when it should also include systematic checks, accelerator configuration change, spin dance, and calibrations. These activities required 10% of the beam time during the G0 forward angle production run. On the other hand, optimization of the target position for the backward angle production runs seems to balance this. A breakdown of the beam time between the production data (with the statistical goal) and the ancillary data taking is required.*

We estimate that about 10% of the beam time available for this measurement will also be used for such measurements as shown in Table 3.2. These estimates are based on our experience running the forward angle measurement. In addition, we plan to make an initial beam polarization measurement to check the Møller calibration and electronic deadtimes at low energies (1.2 d).

3. *The beam time request mentions high beam polarization. The call for proposals states a maximum beam polarization of 75%. Is this what is assumed?*

Yes, 75% is what we were directed by the lab to use. This should be safe as we will run this measurement with the standard 499 MHz beam structure.

4. *The proposal assumes a higher efficiency (60% instead of 50%) for the beam time request at a 360-MeV beam energy under the assumption that this will be a single-hall*

experiment.

We believe this is a point of information - this is the efficiency we were asked by the lab to assume.

5. *A beam energy of 360 MeV is very low compared to the usual CEBAF operating mode. Apart from the technical aspects of delivering such a low energy, the issues related to the experiment itself could be more developed.*
 - (a) *There is no estimation of the level of radiation (and therefore the anode current in the PhotoMultiplier Tubes). It is unclear that the shielding scheme developed for the 0.799 GeV run would suffice for the lower energy run.*

The results from our ‘Hall’ simulations using a combination of the Geant code used by the Radiation Control Group (P. Degtiarenko) and our G0Geant geometry are discussed in detail in Section 1.2.2 of the update. These calculations have been performed explicitly for both hydrogen and deuterium running at 360 MeV.

- (b) *The proposal states that the helicity-correlated beam properties already achieved during the forward angle running (at a 3 GeV energy) are more than sufficient for the back angle running. Given the potential difficulties to tune the beam at these very low energies, an updated beam specification table with minimal beam parity-quality requirements is essential.*

The beam specifications for this run are discussed in detail in Section 2.1 of the update. They have been communicated to and discussed in detail with the Accelerator Division. Also of note in this context is the appointment of Dr. Joe Games as the specific representative of the Accelerator Division for the installation and operation of the backward angle phase of the experiment.

- (c) *The beam spot size for such low-energy experiments may be drastically enhanced in the Hall C beam line. The collaboration needs to develop a realizable beam halo specification for these low beam energies.*

The halo issues for this run are discussed in detail in Section 1.2.1 of the update. This discussion has been developed in consultation with various accelerator experts who are members of our collaboration (J. Games, J. Benesch, M. Poelker, R. Kazimi).

6. *Given the anticipated worse beam quality at 360 MeV, a beam period with collaborative tests to demonstrate feasibility of the beam specifications both in the injector region and in the Hall C beam line is required.*

We agree completely. In the past we have actively pushed for more accelerator

test time prior to our runs, the overall pressure on beam time has often reduced to inadequate levels the time available for getting the accelerator ready. We have been in contact with Andrew Hutton, and discussed the setup for both 687 MeV beam and that at 360 MeV. We agree on the need for adequate time for this type of preparation, especially for 360 MeV. We would be grateful for any support you can give us in this regard.

7. *The proposal seems to be written as if the experiment precision was purely statistic. In this case, the experiment seems to aim at a 2% measurement of the asymmetries for both of the Q2 (in the case it is decided to run with hydrogen only). No systematic errors on the extracted elastic asymmetries seem to be taken into account beside some nuclear corrections in the case of the deuterium target and the polarimetry precision. In particular:*

- (a) *The collaboration assumes that moving the Møller quadrupole upstream from its usual position would be enough to accommodate the very low energies. The optics calculations for this configuration need to be tested in-situ. The test can be performed during the 0.799 GeV run. If the Møller can be used in this configuration, the precision on the resulting polarization measurement need to be evaluated: It could easily double the beam polarization uncertainty assumed in the proposal. Is there a back-up plan in case the Møller cannot be used?*

We expect the systematic uncertainties to be dominated by those from the polarization measurement and from the background correction. The beam polarization has been measured with the Hall C Moller polarimeter at around 900 MeV in the GEn experiment by moving one of its quadrupole magnets downstream. Dave Gaskell has investigated this configuration at 360 MeV (with a slightly larger quadrupole shift) and has found an acceptable solution. It is likely that this configuration will require a cross check for calibration. In this regard we note that the 5 MeV Mott polarimeter (Joe Grames is the expert) now provides a very good measure of the polarization and, at this low beam energy with minimal bending of the beam, we are investigating the possibility of using it to help provide a calibration. Lastly, in the proposed transition from 687 MeV (both linacs) to 360 MeV (same setup but one linac) running, the maximum beam polarization should not change - providing a good starting point for the measurement (and, if necessary, we could in principle go back to 687 MeV to check during the tuneup). We assumed $75 \pm 2.4\%$ for the beam polarization in the proposal; if this uncertainty increases it could dominate the uncertainties and we will work to be sure its impact is minimized.

- (b) *The proposal is missing a clear discussion of how the elastic asymmetry will be isolated from the coarse 2-dimensional matrix of scalar information, and what the impact of this separation on the final errors would be. This should be done, even if with some simplifying assumptions, for both the yields and asymmetries.*

This issue is addressed in detail in Sections 2.3 and 4.1 in the update. We note

that for this measurement, the inelastic electron contamination in the detector combinations with the elastic yield is $< 1\%$. We have, however, conservatively assumed a (smooth) background of as much as $\sim 10\%$ over all detectors in making the uncertainty estimates in Section 2.3.

8. *Due to multiple scattering, the beam diameter at the Hall C beam dump will be of order 50 cm diameter, assuming a 360 MeV beam passing through a 4% radiation length target. The result is that much of the beam power will be deposited upstream of the 30 cm diameter beam dump face. The effect of this on the site boundary radiation dose, the detector backgrounds, and dump line equipment must be investigated.*

These issues have been addressed by the laboratory Radiation Control Group and there is consensus that the present dump is adequate for this measurement and that the radiation produced is acceptable from the Laboratory point of view. As discussed above and in Section 1.2.2, we have also developed a shielding configuration to reduce the background effects on our detectors to an acceptable level.

9. *Secondly, please summarize the pros and cons of focusing on $Q^2=0.23$ vs $Q^2=.48$ and having or not both 1H and 2H targets, thereby making a separation of GMs and GA possible.*

This issue is addressed for the $Q^2 = 0.23 \text{ GeV}^2$ case in Section 4.1. We are proposing to run both hydrogen and deuterium targets with the time split to give the best possible combined measurement for G_E^s , G_M^s and G_A^e (optimum is equal times for the two targets). We will subsequently address the question of whether to propose another measurement based on the results of the $Q^2 = 0.63$ and 0.23 GeV^2 experiments.

B Appendix: Beam parameter specifications for the G^0 experiment (Backward Angle Running)

Beam Parameter Specifications for the G^0 Experiment (Back Angle running)

From: R. Carlini, S. Page, M. Pitt for the G^0 collaboration

To: Hari Areti, Matt Poelker, Michael Tiefenback

Date: December 17, 2001; updated by Mark Pitt (Oct. 7, 2005) for back angle running; updated again by Mark Pitt on Oct. 25 and Nov. 30

This is our response to the request for a beam parameter specification sheet for the G^0 experiment in its backward angle mode of running. The parameters and discussion in this document are for the most part identical to that in the document we provided the lab for the forward angle run. Here is a summary of the major changes:

1. The beam time structure will be the normal 499 MHz time structure (rather than the 31 MHz time structure from the forward angle run. The maximum desired current will be 100 μ A, while the nominal current will be 80 μ A.
2. The requirements on maximum allowed run-averaged helicity-correlation for energy, angle, current, and position have been relaxed by a factor of 2 relative to the forward angle run. This is primarily because the measured asymmetries in the back angle mode are larger than those for the forward angle mode.
3. The discussion of “betatron match” or “adiabatic damping” in point 11 has been updated to reflect the numbers observed during the forward angle running. We continue to support any development time that can be given to Y. Chao for further understanding and control of this issue.
4. A new point (point 12) has been added for further clarification of our requirements regarding beam halo.

Our beam property requirements are summarized in Table 1. For each beam property, we list requirements in the categories defined below. Some of the beam requirements are taken directly from a table prepared (10/31/01) by J-C. Denard that summarized the work of the committee that recently determined standard parameters for beam delivery.

Categories:

1. **Nominal value:** This is the usual desired central value of the beam property.
2. **Maximum deviation from nominal (DC):** This is how far the DC (averaged over several seconds; ie. EPICS update timescale) central value of the beam property can drift from the nominal value before corrective action is required.
3. **Maximum noise at the helicity reversal frequency:** Operationally, we integrate the signal from any given beam property over a 33 msec time period. Then we form differences between two successive 33 msec integration periods. The standard deviation of the distribution of those differences is what we refer to as the “noise at the helicity reversal frequency”. It needs to be kept small enough so that we can measure helicity-correlated position differences and current asymmetries accurately enough to do feedback. The values quoted in the table are already typically

achieved, with the exception of the current stability with the G^0 laser which is not known yet.

4. **Maximum noise at all other frequencies:** This is the upper limit on the random noise in a given beam property at frequencies other than the helicity reversal frequency. (for example, 60 Hz noise and higher harmonics)
5. **Maximum allowed run-averaged helicity-correlation:** This refers to the maximum value of the helicity-correlated difference (or asymmetry) that can be tolerated in that beam property after averaging over the entire 700 hour run. This assumes that injector-based helicity-correlated feedback systems will be in place to achieve these values. We are participating with the injector group to develop and test systems to do this prior to our run. It should be noted that the run-averaged values listed in the table were achieved during the 1999 HAPPEX run with a strained GaAs crystal.

To clarify this category a little better, we consider the specific example of helicity-correlated differences in the beam position. Assuming that the fluctuations in the beam position at the reversal frequency are 20μ , we can determine the helicity-correlated beam position difference in a 1 hour run with a precision of ± 86 nm. The feedback system for this (piezoelectric mirror) would likely be updated on this timescale. If we then look at the distribution of all 700 one hour long helicity-correlated position differences measurements at the end of the run, it would roughly be a Gaussian with a centroid that is less than the number in Table 1 (< 20 nm) and a standard deviation around 86 nm. So it is difficult to specify a “maximum tolerable” position difference in 1 hour, since statistics dictates that there will occasionally be a large one by chance. One needs to average the data over a reasonable timescale (say 8 hours) to determine if we have a problem that needs corrective action.

Table 1: Beam property specification table for G^0 . Definition of the various categories can be found in the text.

Beam Property	Nominal value	Maximum deviation from nominal (DC)	Maximum noise at the helicity reversal frequency	Maximum noise at all other frequencies	Maximum allowed run-averaged helicity-correlation
Energy(average)	360, 687 MeV	$\pm 0.1 \%$	0.001% (35μ at 35mm/%)	0.01% (350μ at 35 mm/%)	$< 5 \times 10^{-8}$ 180 nm at 35 mm/%
Energy spread (1σ)	$\sigma_E/E < 1 \times 10^{-3}$	$\sigma_E/E < 1 \times 10^{-3}$			
CW average current	80 μ A	$\pm 5.0 \%$	0.2%	1.0%	< 2 ppm
Position at G^0 target	“0”	± 0.2 mm	20 μ	0.2 mm	< 40 nm
Angle at G^0 target	“0”	± 0.050 mr	2 μ r	0.02 mr	< 4 nr
Angular divergence at G^0 target	$\sigma_x, \sigma_y < 100 \mu$ r	$\pm 50\%$			
rms size (unrastered) at G^0 target	$< 200 \mu$	$\pm 25\%$	20 μ	0.2 mm	$< 4 \mu$
Polarization	$> 70\%$				
Beam halo at G^0 target	$< 1 \times 10^{-6}$ outside of a 3 mm radius				$< 0.2\%$ of nominal halo tolerance

Other considerations and clarifications:

1. **Basic beam tune:** The tune should be achromatic at the target (< 1 mm/% dispersion) with large enough dispersion (35 mm/%) at the center of the Hall C arc to make an accurate relative energy measurement.
2. **Raster pattern:** The raster for G^0 is being developed by Chen Yan. The current specifications call for a square pattern with raster frequencies of $f_x=25$ kHz and $f_y=25.02$ kHz. The maximum length per side of the square is 3 mm.
3. **Helicity-defining Pockels cell:** The laser arrangement should be set up so that the Hall C beam is on the center of the Pockels cell, and the Pockels cell should be adjusted to provide the maximum possible circular polarization for the Hall C beam.
4. **Rotateable half-wave plate:** The rotateable half-wave plate should be set to the value that minimizes the Hall C current asymmetry when no other helicity-correlated feedback systems are turned on.
5. **Stability of electron beam polarization:** As is well known, there have been issues associated with measuring the electron beam polarization at different beam currents. These arise from the way the laser beams are combined and leakage currents from one hall to another. Whether any such issues will exist for the G^0 time structure is unclear at this point. It will be important to assess the situation when we have beam to determine if there is any situation like this that will compromise our experiment's ability to determine the beam polarization with a relative precision of $\pm 2\%$.
6. **Cross-talk with other halls:** There are two possible categories of cross-talk of other hall's beams into the Hall C beam:
 - a. Current leakage: We want the contribution of the summed beam currents from other hall's beams to be less than 1% of the Hall C beam current.
 - b. "Helicity-correlated" leakage: It has been observed during HAPPEX running in 1999 that a helicity-correlated intensity in another hall's beam can induce helicity-correlated energy and position differences in their beam. The exact origin of this was not determined, but the solution is to have helicity-correlated feedback controls on the other hall's lasers. This will need to be done to the extent that it is necessary to satisfy the helicity-correlation specifications in Table 1.
7. **Helicity-correlated feedback systems:** For helicity-correlated feedback systems at the polarized injector, we prefer that each laser beam have separate helicity-correlated feedback controls. We prefer that devices that are common to all laser beams (the helicity-defining Pockels cell and the rotateable half-wave plate) not have active feedback on them, and they should only occasionally be adjusted while keeping to the guidelines in points 2 and 3.
8. **Fast energy and position locks:** Our experience during the forward angle run was that it was best for us to run with these systems off.
9. **Beam position and angle modulation:** We will be using air core steering coils in the Hall C beamline upstream of the arc to modulate the beam position and angle at the G^0 target over ranges of ± 1 mm and ± 1 mr, with the timescale for changes being ~ 200 -300 msec. This type of modulation was done during both HAPPEX runs, so the protocols for safety have been thought out before, and we will follow them. The

frequency for runs of this type has not yet been determined, but it could be as often as once per hour.

10. **Beam energy modulation:** This system was in use during HAPPEX to modulate the beam energy by varying a cavity in the South Linac. This affects the other halls beams, as well, but it was done routinely during HAPPEX running. The frequency for runs of this type has not yet been determined, but it could be as often as once per hour.
11. **Betatron match:** While this is still an area of active development, we request that the accelerator tune be “betatron-matched” as well as the current accelerator instrumentation allows. We are interested in this because of the adiabatic damping effect that can suppress helicity-correlated position differences in the experimental hall. Our main diagnostic for this is the comparison between the size of helicity-correlated position differences in the experimental hall versus the 5 MeV region of the injector. We will be able to monitor this ratio continuously when we are running. It will be useful to see if there is a correlation between this diagnostic and the accelerator measurements of the Courant-Snyder parameters. Suppression factors of ~ 10 were observed for the forward angle run. In principle, the adiabatic damping should be much better than this. Most of the loss of adiabatic damping appears to be in the injector region. We support the continued efforts of Y. Chao to understand and improve this situation.
12. **Beam halo specification:** There are two ways that significant beam halo could potentially be problematic for the experiment. They are:
 - **Interaction of beam halo with the thick parts of the G^0 target flange:** The specification in the table ($< 1 \times 10^{-6}$ outside of a 3 mm radius) primarily comes from the fact that we want to minimize the interaction of any part of the beam with the thick parts of the G^0 target flange (which start at a radius of 5.5 mm). During the forward angle run, we monitored this specification by continuously running with an aluminum target (2 mm thick) with a 6 mm diameter hole in it located about 8 meters upstream of the G^0 target. Downstream of this hole target there were PMTs with scintillators at large (15 degrees) and small (3 degrees) angles. We calibrated the system by putting 5 nA of beam directly into the 2 mm thick part of the aluminum halo target. From this, we could directly show that the above specification was being achieved, and we monitored it continuously during running. The specification was routinely achieved (for the potentially more problematic 31 MHz beam) except in some cases where the tune suddenly went drastically bad, and usually there was a clear cause why things had gone bad.
 - **Interaction of the beam halo with some small upstream aperture:** The potential problem here is that beam halo interacting with a small upstream aperture could generate background that gets detected in our scintillators. This could either cause higher PMT anode currents than we can live with or contribute a background to our coincidence count rate. To measure this, we remove the main G^0 target and the halo target entirely. During the forward angle run, this rate was completely negligible. But during the forward angle running the scintillation detectors were downstream of the magnet, which provided some protection against backgrounds of this type. In the backangle mode of running, the detectors are upstream of the magnet, so they do not have this protection. To attempt to set a (crude) specification here, we would need to

know where the smallest upstream aperture in the beamline is, what material it is made of, and how thick it is. Then we could make some estimates of what fraction of the beam could hit that aperture before it created problems for our scintillation detectors downstream in the experimental hall.